# Supporting Information

# Superhydrophilic Porous CoOOH Nano-Architecture with Abundant Oxygen Vacancies for Enhanced Urea Electrooxidation at Ampere-Level Current Densities

Wenjing Lv, Xiaoman Tang, Xuetong Wang, Wencai Liu, Jianwen Zhu, Guojing Wang* and Yuanzhi Zhu*

Faculty of Chemical Engineering, Yunnan Provincial Key Laboratory of Energy Saving in Phosphorus Chemical Engineering and New Phosphorus Materials, Kunming University of Science and Technology, Kunming 650500, Yunnan, China.

E-mail: gjwang@kust.edu.cn; yuanzhi_zhu@kust.edu.cn

## Experimental Section

**Materials.** Cobalt(II) nitrate hexahydrate ($Co(NO_3)_2·6H_2O$, ≥98%), urea ($NH_2CONH_2$, 99%), acetone ($CH_3COCH_3$, 99%), nitric acid ($HNO_3$, 68–70%) and potassium hydroxide (KOH, >99%) were commercially available from Sinopharm Chemical Reagent Co., Ltd.. Ammonium fluoride ($NH_4F$, 98%) and sodium hypophosphite monohydrate ($NaH_2PO_2·H_2O$, 98%) were purchased from Aladdin Chemistry Co., Ltd.. Carbon fiber paper (CFP, ~180 μm in thickness) were ordered from Wuhan Cetech Co., Ltd.. All reagents were used without any further purification. Deionized water (18.2 MΩ) produced from a Milli-Q purification system was used for the samples synthesis and electrochemical measurements. CFP was thoroughly washed by sonication in acetone and water for 15 min respectively and then pretreated with nitric acid (68–70%) at the 75 °C for 90 min to achieve the surface hydroxylation of CFP. After being washed with deionized water, the pretreated CFP was used as the substrate for the syntheses of various integrated catalysts.

## Characterization of materials

Scanning electron microscopy (SEM) were carried out using a Hitachi SU-8010 field-emission scanning electron microscope operating at an acceleration voltage of 5 kV to probe the morphology of the catalysts. Transmission electron microscopy (TEM) images, High-resolution TEM (HRTEM) images, scanning TEM (STEM) images, and EDX elemental maps were obtained using an FEI Talos F200S transmission electron microscope accompanied by two energy disperse X-ray spectrometers (Super-EDS) operated at 200 kV. The specimens for TEM observations were carefully scratched from the CFP support and sonicated fully before dropping them onto ultrathin carbon-coated copper grids with 200 mesh. X-ray photoelectron spectroscopy (XPS) measurements were performed using a ESCALAB 250Xi spectrometer

with a hemispherical energy analyzer, employing a monochromatized microfocused Al-Kα (hv = 1486.58 eV) X-ray source to analyze the surface composition and chemical states the catalysts. The binding energies (BEs) of the core levels were calibrated by setting the adventitious C1s peak at 284.8 eV. The X-ray diffraction (XRD) patterns were collected using a Rigaku SmartLab diffractometer equipped with a Cu Kα X-ray source (λ = 1.5406 Å), operating at 40 kV and 100 mA at a scanning rate of 0.06° $s^{-1}$ from 10 to 90°. Electron paramagnetic resonance (EPR) analyses were conducted on a Bruker EMX PLUS. The elemental composition of the samples was determined by EDX quantitative analysis and inductively coupled plasma atomic emission spectrometry (ICP-AES, Prodigy, Leeman Labs Inc., λ = 165–800 nm, As = 200 nm) measurements after dissolving the sample in aqua regia. The Wettability test was conducted on contact angle measurement instrument (Dataphysics OCA 20). The photos of bubbles release were obtained by a high-speed charge-coupled device camera (Phantom Miro 320s). The gas products ($N_2$ and $CO_2$) formed during electrolysis were analyzed by on-line gas chromatography with Haixin GC 950 gas chromatography system. Ion chromatography (IC) was conducted on Metrohm 883 Basic IC plus.

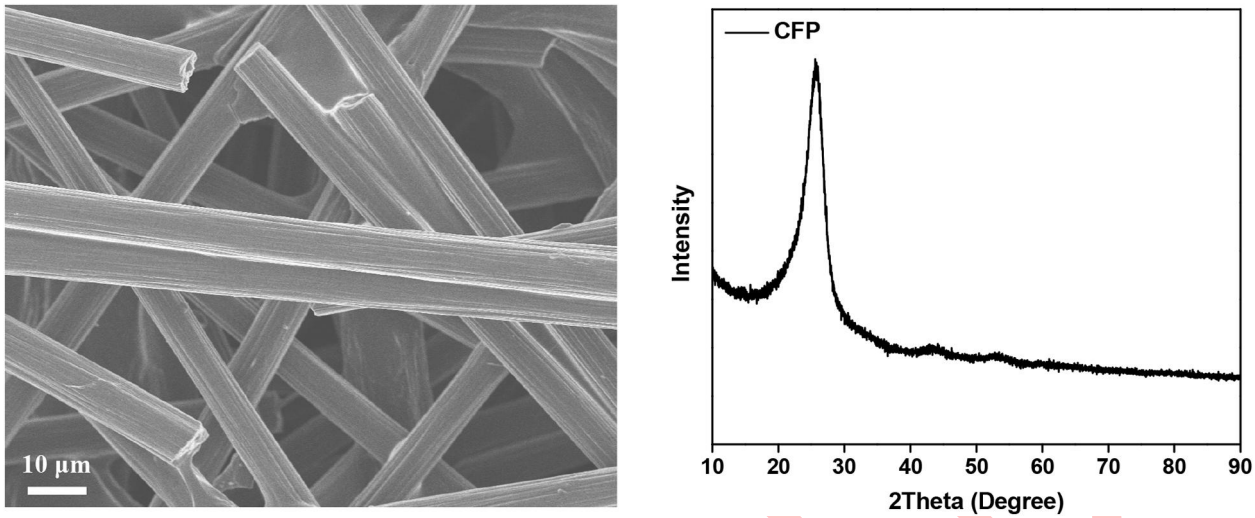


**Figure S1.** (a) SEM image and (b) XRD pattern of Carbon fiber paper (CFP).

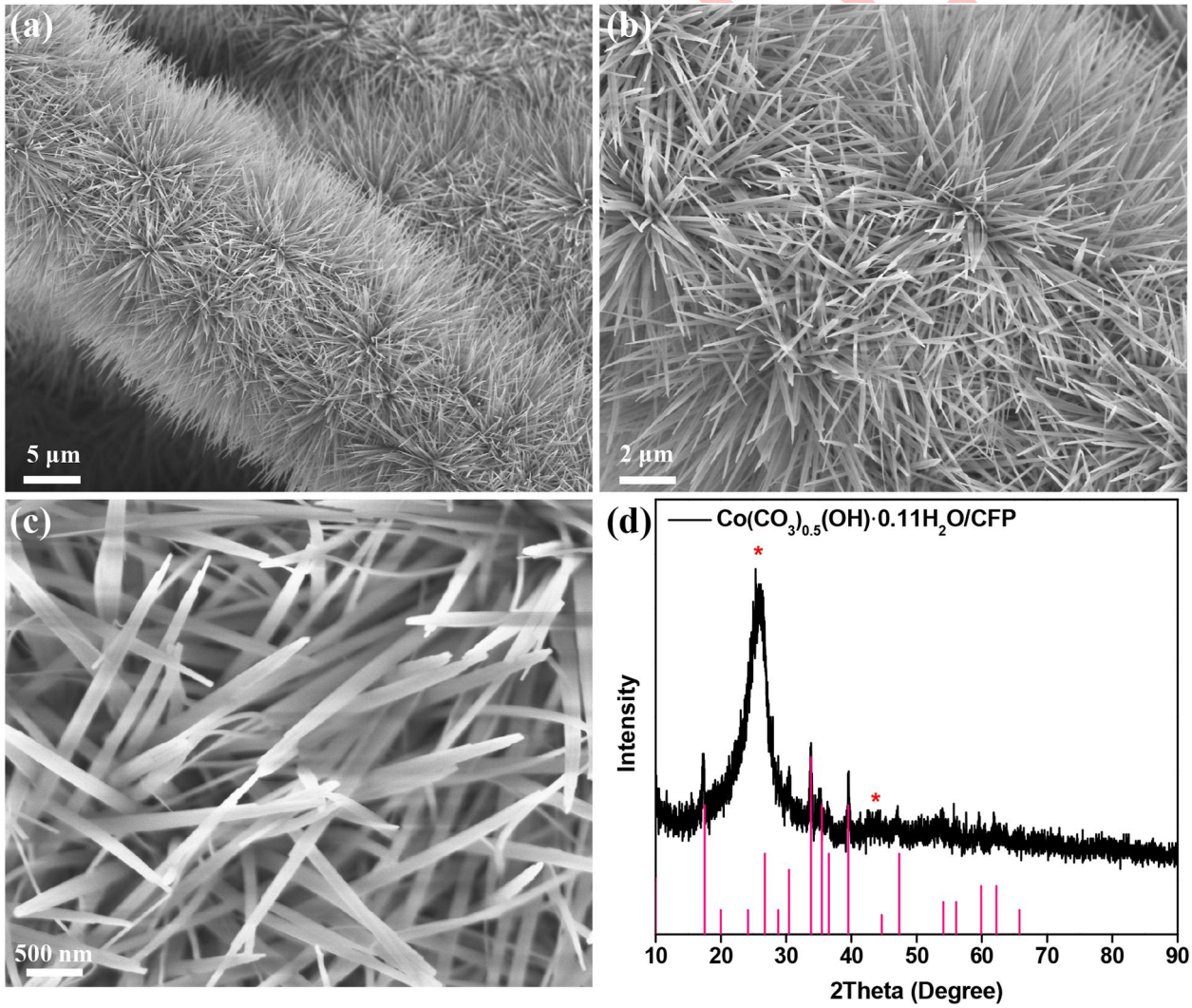


**Figure S2.** (a, b) SEM, (c) TEM images and (d) XRD pattern of the $Co(CO_3)_{0.5}(OH)\cdot 0.11H_2O$ NNs/CFP.

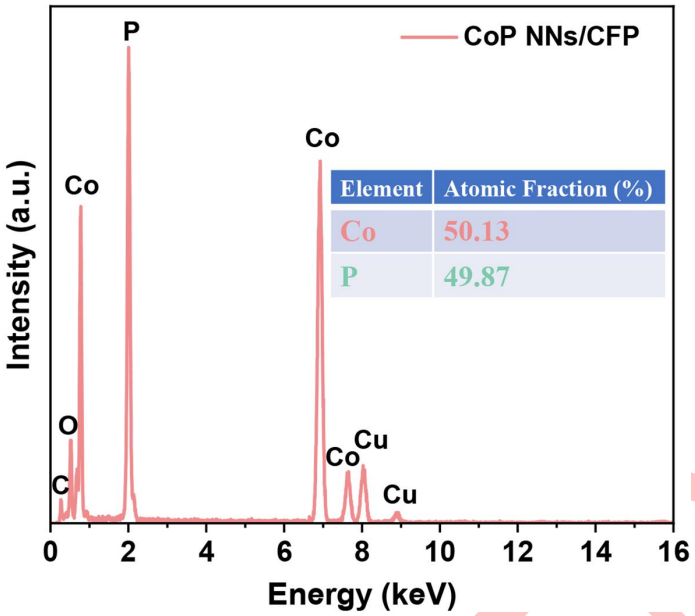


**Figure S3.** EDX spectra of the CoP NNs/CFP.

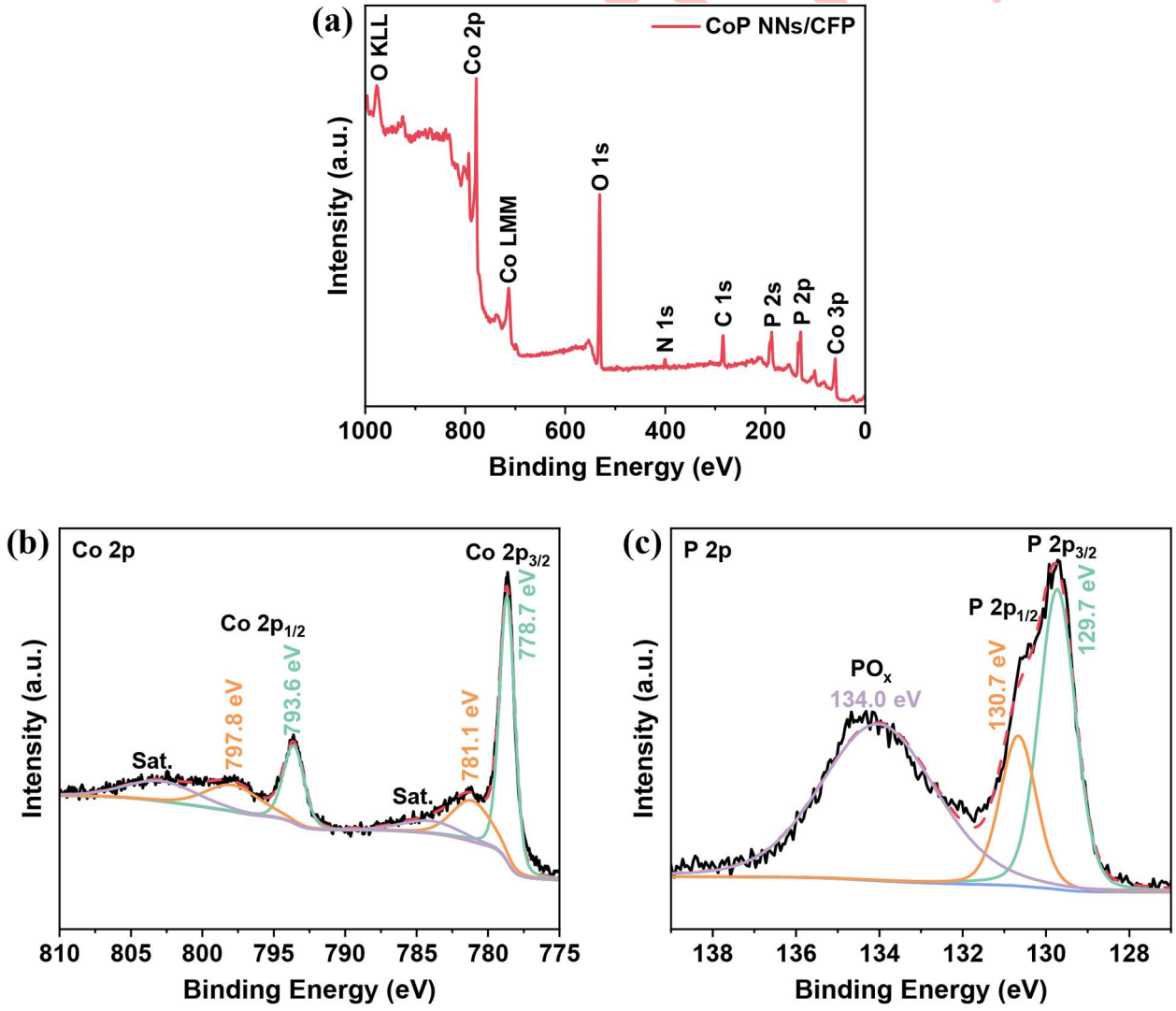


**Figure S4.** (a) The XPS survey spectrum and the high-resolution (b) Co 2p and (c) P 2p XPS spectra of the CoP NNs/CFP.

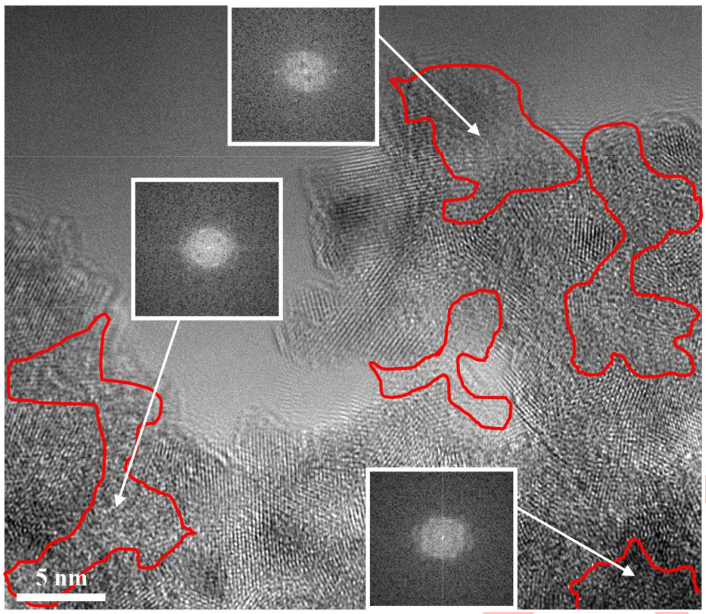


**Figure S5.** HRTEM image of the CoOOH LPNAs/CFP. The insets show the corresponding fast Fourier transform (FFT) patterns.

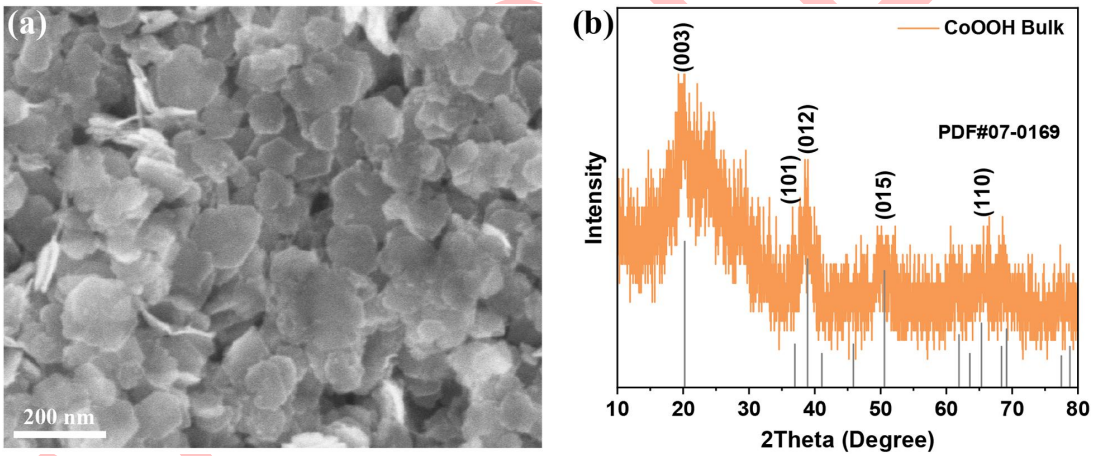


**Figure S6.** (a) SEM image and (b) XRD pattern of CoOOH bulk.

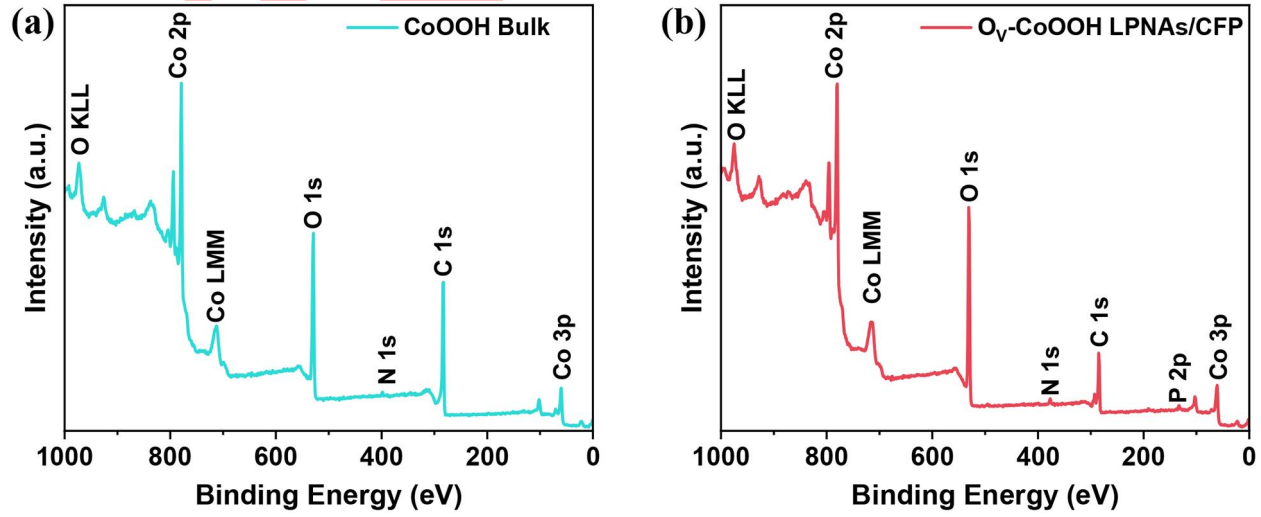


**Figure S7.** The XPS survey spectrum of (a) CoOOH bulk and (b) CoOOH LPNAs/CFP. The XPS survey spectrum of CoOOH LPNAs/CFP shows a very weak P characteristic peak. According to the XPS characterization results, the Co/P atomic ratio is determined to be 34.5:1, indicating that only a trace amount of phosphorus remains in the CoOOH structure.

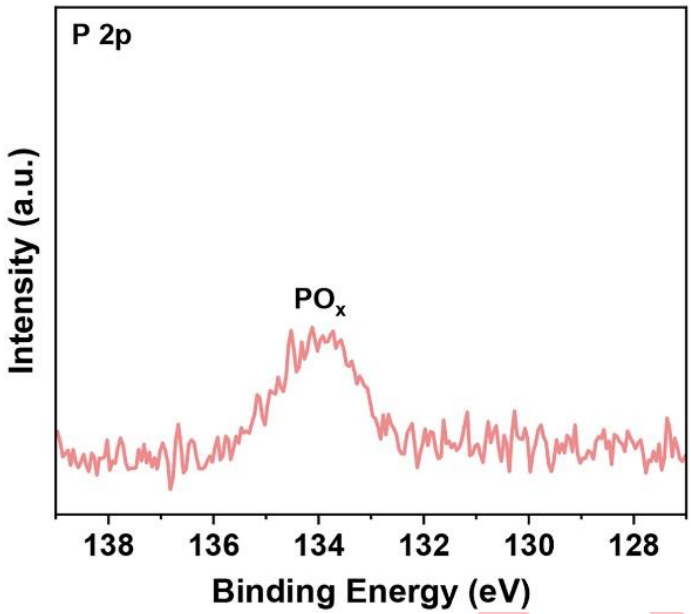


**Figure S8.** High-resolution P 2p XPS spectra of CoOOH LPNAs/CFP. High-resolution P 2p XPS spectrum shows that the Co–P bonds have completely disappeared, and only a weak $PO_x$ signal is detected. This suggests that the residual phosphorus does not incorporate into the CoOOH lattice as dopants but rather exists as surface-bound $PO_x$ species. The trace amount of $PO_x$ (approximately 0.98% of P atomic % in CoOOH) is unlikely to significantly influence the electronic structure and catalytic performance of the material.

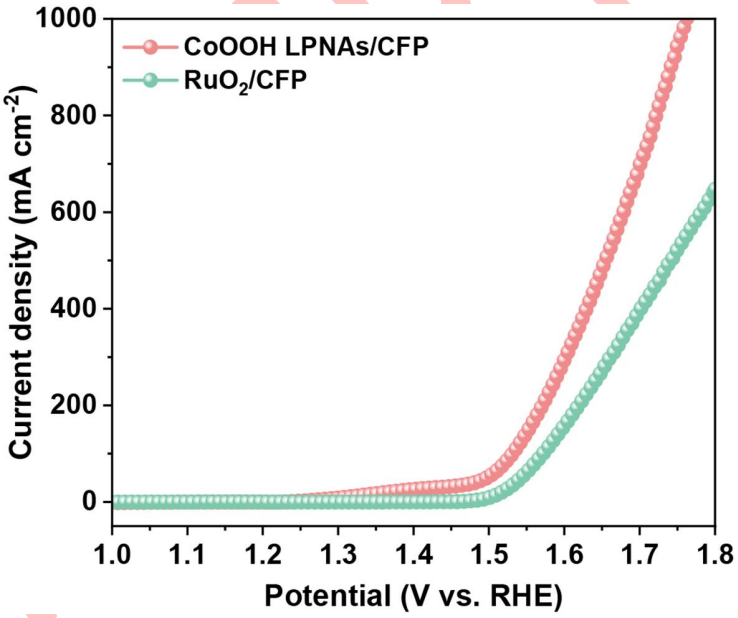


**Figure S9.** Polarization curves of CoOOH LPNAs/CFP and $RuO_2$/CFP for OER recorded in 1 M KOH.

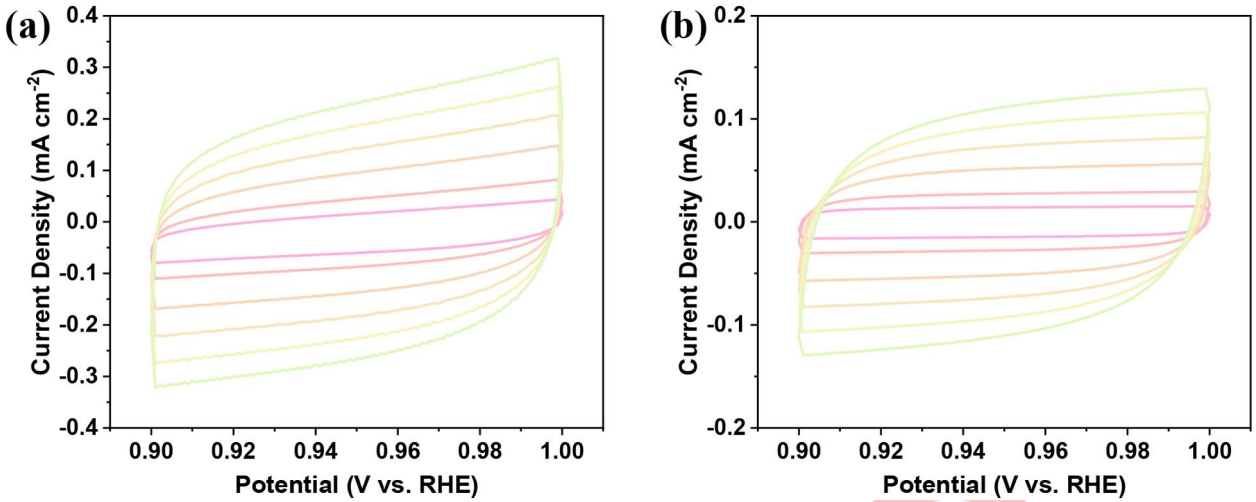


**Figure S10.** Cyclic voltammograms of the (a) CoOOH LPNAs/CFP and (b) CoOOH bulk/CFP electrodes, which are used to estimate the double layer capacitances ($C_{dl}$). Sweep rates at 10, 20, 40, 60, 80 and 100 mV $s^{-1}$ were chosen.

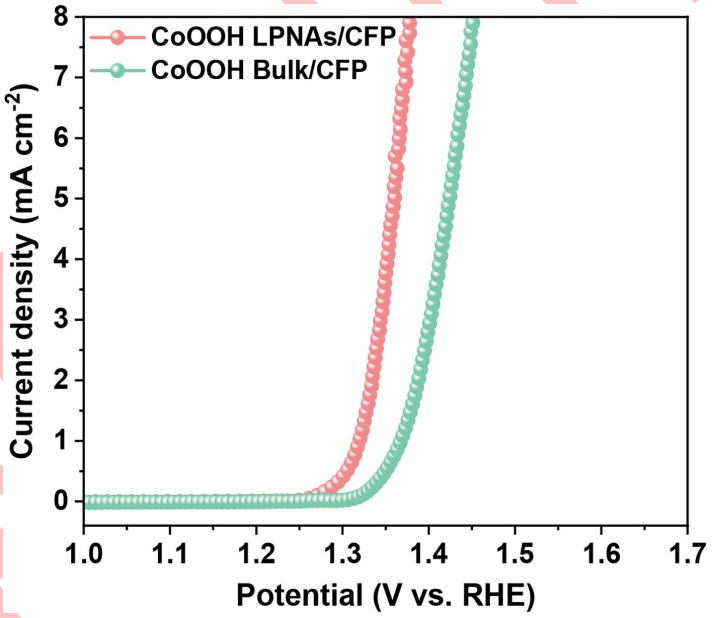


**Figure S11.** Specific activity based on ECSA of the CoOOH LPNAs/CFP and CoOOH bulk/CFP.

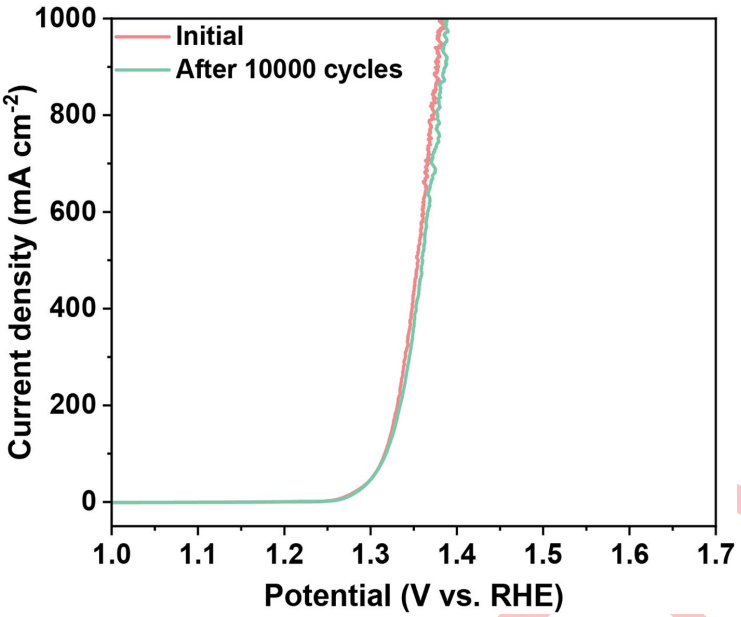


**Figure S12.** Polarization curves of CoOOH LPNAs/CFP corresponding to the 1st and 10000th potential cycle recorded in 1 M KOH with 0.33 M urea.

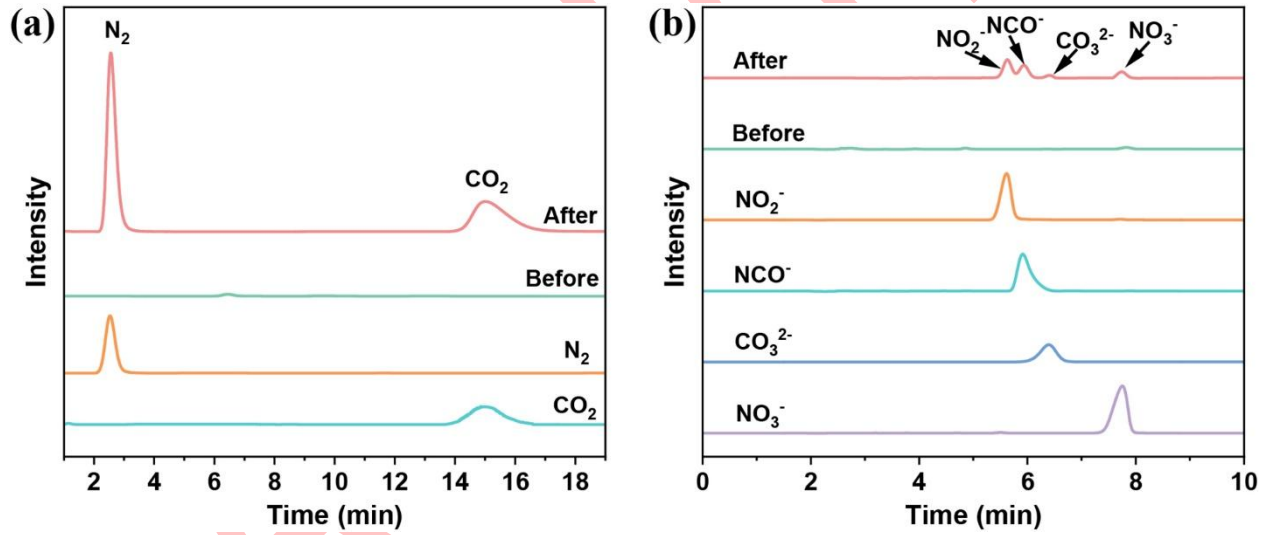


**Figure S13.** (a) The GC trace of the mixture after the UOR reaction recorded by CoOOH LPNAs/CFP, as compared to several standard gases. (b) The IC trace of the mixture after the UOR reaction recorded by CoOOH LPNAs/CFP, as compared to several standard ions.

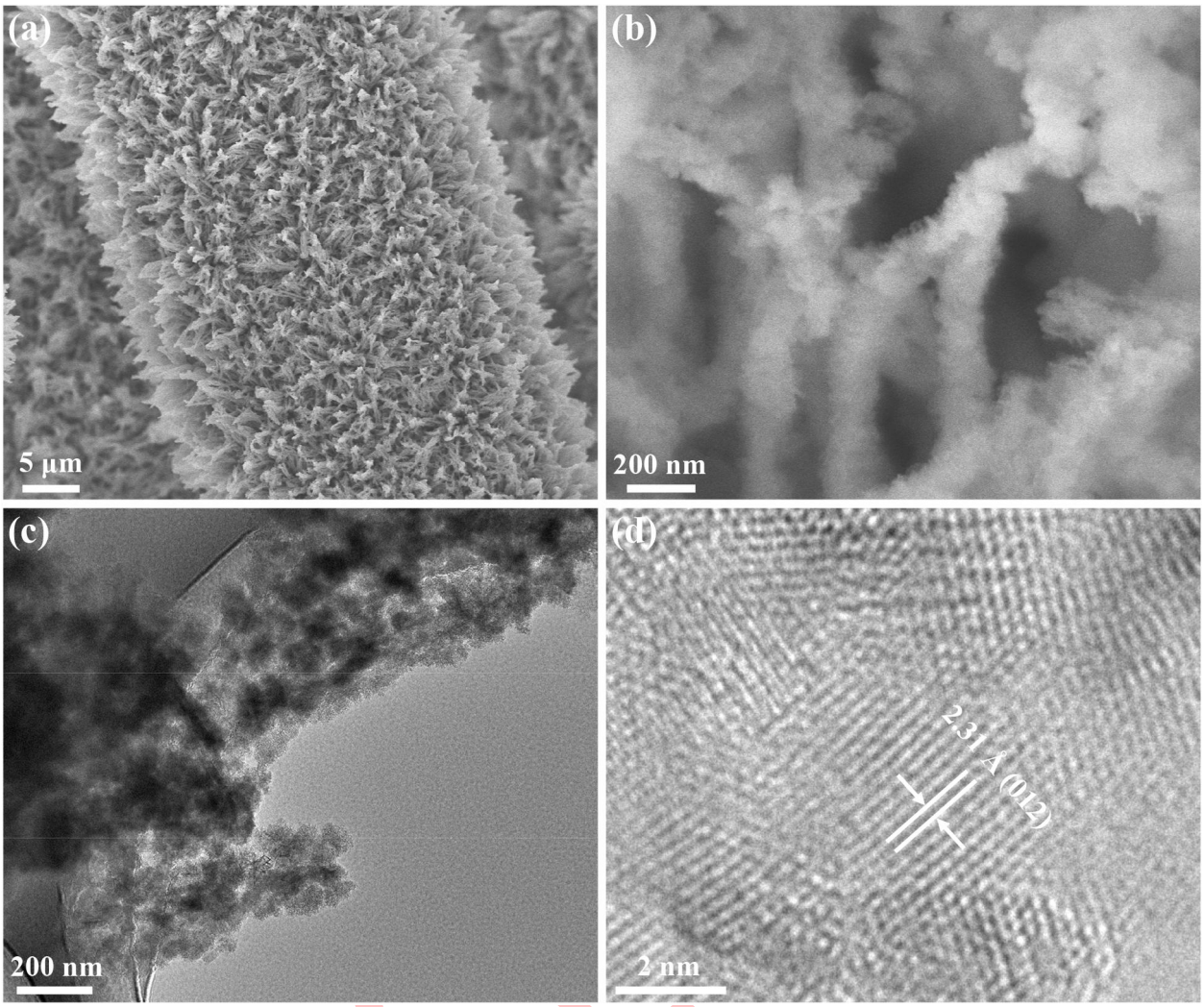


**Figure S14.** (a, b) SEM, (c) TEM and (d) HRTEM images of the CoOOH LPNAs/CFP after a stability test for 200 h.

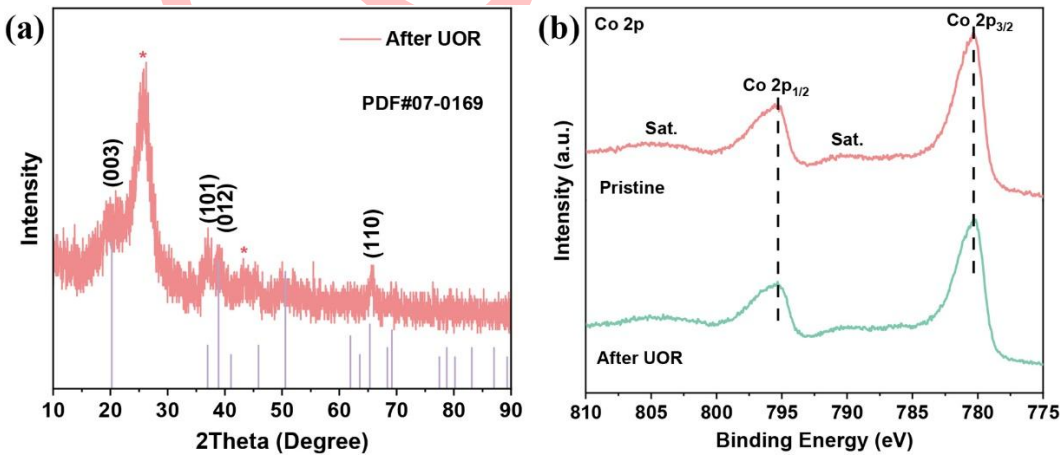


**Figure S15.** (a) XRD spectra and (b) high-resolution Co 2p XPS spectra of the CoOOH LPNAs/CFP after a stability test for 200 h.

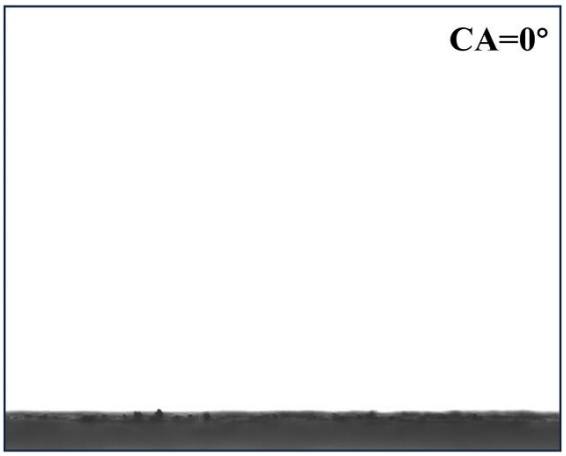


**Figure S16.** The wettability test of CoOOH LPNAs/CFP after a stability test for 200 h.

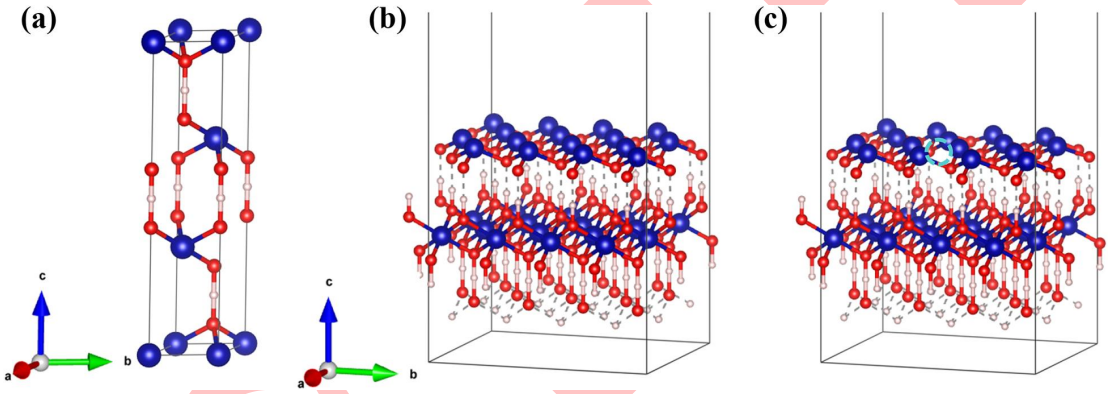


**Figure S17.** The geometric structures of (a) CoOOH unit cell, (b) slab model for CoOOH (001) facet and (c) slab model for $O_v$-CoOOH (001) facet.

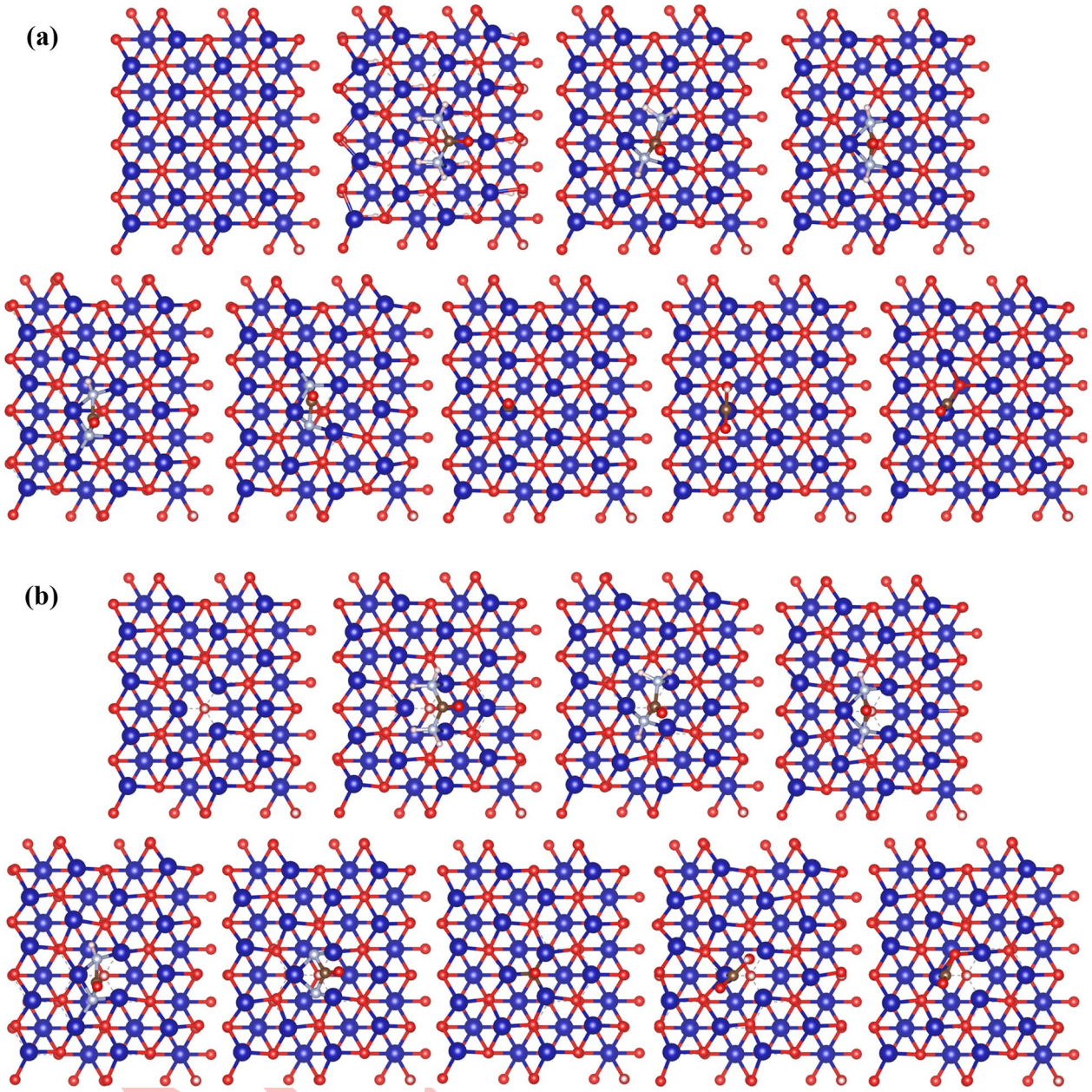


**Figure S18.** The side views of schematic models of UOR elementary steps on (a) CoOOH (001) and (b) $O_v$-CoOOH (001). The pink, red, and blue spheres represent H, O, and Co atoms, respectively.

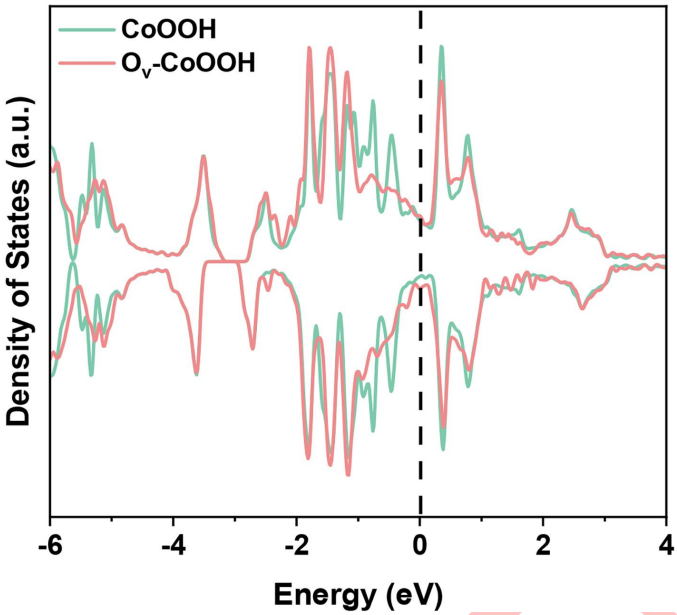


**Figure S19.** Total DOS on CoOOH (001) and $O_v$-CoOOH (001) surfaces.

**Table S1.** Comparison of the electrocatalytic activity of various non-noble metal-based catalysts in the literature with CoOOH LPNAs/CFP in this work for the UOR in alkaline electrolyte.

| Catalysts | Electrolyte | $E_{100}$ (V) | $E_{1000}$ (V) | Tafel slope (mV dec$^{-1}$) | Ref |
|---|---|---|---|---|---|
| **CoOOH LPNAs/CFP** | **1 M KOH+0.33 M urea** | **1.32** | **1.38** | **48** | **In this work** |
| β-Ni(OH)$_2$-S/CuNDs | 1 M KOH + 0.33 M urea | 1.36 | — | 27 | *Chem. Eng. J.* 2024, **490**, 151251 |
| CoNi-LDH/Fe MOF/NF | 1 M KOH + 0.33 M urea | — | 1.49 | 50.7 | *ACS Appl. Mater. Interfaces* 2024, **16**, 14742−14749 |
| NiMn-MOF | 1 M KOH + 0.33 M urea | 1.326 | 1.459 | 34 | *ACS Nano* 2024, **18**, 35654−35670 |
| Ni(OH)$_2$/ACE | 1 M KOH + 0.33 M urea | 1.34 | 1.36 | 16.6 | *Adv. Mater.* 2024, **36**, 2409292 |
| Ru/P-NiMoO$_4$@NF | 1 M KOH + 0.5 M urea | 1.36 | 1.47 | 14.3 | *Appl. Catal. B-Environ.* 2023, **320**, 121977 |
| CoNi@CN-CoNiMoO | 1M KOH + 0.5 M urea | — | 1.4 | 30 | *Carbon Energy.* 2023, **5**, e368 |
| NiO@MoNi$_4$/C | 1M KOH + 0.5 M urea | 1.41@500 | 1.47 | 41.12 | *Small* 2025, **21**, 2410044 |
| Ni$_3$S$_2$@Ni$_3$P | 1M KOH + 0.33 M urea | 1.36 | 1.49 | 19.13 | *Chem. Eng. J.* 2024, **483**, 149264 |
| Ni$_3$Se$_4$-MoSe$_2$/Co@C | 1 M KOH + 0. 5 M urea | 1.367 | 1.427 | 30.2 | *Chem. Eng. J.* 2024, **499**, 156647 |
| PtNC/NiMn-MOF | 1M KOH + 0.33 M urea | 1.329 | 1.485 | 34 | *ACS Nano* 2024, **18**, 35654−35670 |
| NiSe$_2$/NiFe-LDH | 1 M KOH + 0. 5 M urea | 1.364 | 1.447@800 | 34.8 | *Adv. Funct. Mater.* 2024, 2421136 |
| NiCoCr-LDH/NF | 1M KOH + 0.5 M urea | 1.38 | — | 18.61 | *Adv. Funct. Mater.* 2024, **34**, 2401265 |
| MIM@Fe$_{0.1}$-CoNi CH/NF | 1M KOH + 0.5 M urea | 1.42 | — | 48.84 | *Chem. Eng. J.* 2024, **491**, 152023 |
| D-NiFeV-LDHs | 1 M KOH + 0.33 M urea | 1.36 | — | 21.8 | *Chem. Eng. J.* 493 2024, **493**, 152860 |
| Co$_{0.5}$NiS$_2$-Ni$_3$S$_2$/NF | 1M KOH + 0.5 M urea | 1.33 | — | 26.87 | *ACS Sustainable Chem. Eng.* 2024, **12**, 998−1006 |
| V-NiCo@NC/NF | 1 M KOH + 0.5 M urea | 1.31 | 1.43 | 32 | *Chem. Eng. J.* 2025, **507**, 160565 |

| | | | | | |
|---|---|---|---|---|---|
| Cu/Fe-MOFs | 1 M KOH + 0.33 M urea | 1.43 | 1.54 | 27.5 | *Nanomaterials* 2022, **12**, 1916 |
| $Ni_3S_2$–$NiMoO_4$/NF | 1 M KOH + 0.5 M urea | 1.33 | 1.38 | 25.75 | *ACS Appl. Mater. Interfaces* 2022, **14**, 46481−46490 |
| Fe-($Ni_{12}P_5$/$Ni_3P$) | 1M KOH + 0.5 M urea | — | 1.4@800 | 28.2 | *Chem. Eng. J.* 2023, **452**, 139362 |
| Mn-$Ni_2P$ | 1M KOH + 0.33 M urea | 1.316 | 1.46 | 29.61 | *Water Res.* 2024, **253**, 121266 |
| CoMn/CuNiP/NF | 1M KOH + 0.33 M urea | 1.43@500 | 1.51 | 41 | *ACS Appl. Mater. Interfaces* 2024, **16**, 8717−8732 |

**Table S2.** The atomic percentage of Co and O in CoOOH before and after UOR.

| Samples | Co (atom%) | O (atom%) |
|---|---|---|
| **Pristine** | 33.7 | 66.3 |
| **After UOR** | 33.1 | 66.9 |

**Table S3.** Comparison of the performance of AEM water electrolyzers based non-noble metal-based catalysts in the literature with CoOOH LPNAs/CFP||Pt/C/CFP.

| two-electrode system | cell voltage (V) | stability | Ref |
|---|---|---|---|
| **CoOOH LPNAs/CFP‖Pt/C/CFP** | **1.53 V (1 A $cm^{-2}$)** | **100 h (1 A $cm^{-2}$)** | **In this work** |
| Ni-NC@DWC‖Ni-NC@DWC | 1.13 V (100 mA $cm^{-2}$) | 1000 h (100 mA $cm^{-2}$) | *Adv. Funct. Mater.* 2025, **35**, 2414935 |
| ANH‖Pt/C | 1.75 V (400 mA $cm^{-2}$) | 50 h (400 mA $cm^{-2}$) | *Adv. Mater.* 2023, **35**, 2301549 |
| a-NiCu-NF‖a-NiMo-NF | 1.6 V (50 mA $cm^{-2}$) | 120 h (50 mA $cm^{-2}$) | *ACS Sustainable Chem. Eng.* 2024, **12**, 9908−9921 |
| $VO_x$-CoP/NF‖ $VO_x$-CoP/NF | 1.54 V (100 mA $cm^{-2}$) | 48 h (100 mA $cm^{-2}$) | *Nano Energy* 2024, **126**, 109613 |
| MoN-Ni-5‖ MoN-Ni-5 | 1.53 V (100 mA $cm^{-2}$) | 220 h (500 mA $cm^{-2}$) | *Adv. Funct. Mater.* 2024, 2421222 |
| V-Ni$(PO_3)_2$/$Ni_2P$ ‖ V-Ni$(PO_3)_2$/$Ni_2P$ | 1.61 V (550 mA $cm^{-2}$) | 700 h (100 mA $cm^{-2}$) | *J. Colloid Interface Sci.* 2025, **680**, 665–675 |
| Mo-NiS‖Mo-NiS | 2 V (1 A $cm^{-2}$) | 24 h (100 mA $cm^{-2}$) | *Adv. Funct. Mater.* 2023, **33**, 2210656 |
| 2D $CoSe_2$/$Ni_{0.85}Se$‖Pt/C | 1.91 V (1 A $cm^{-2}$) | 120 h (500 mA $cm^{-2}$) | *Appl. Catal. B-Environ.* 2024, **352**, 124013 |
| NiO/$Co_3O_4$‖NiCoP | 1.94 V (600 mA $cm^{-2}$) | 144 h (600 mA $cm^{-2}$) | *Nano-Micro Lett.* 2025, **17**, 159 |